Stochastic Environmental Research and Risk Assessment (2018) 32:733–748
https://doi.org/10.1007/s00477-017-1491-z

ORIGINAL PAPER

Singular value decomposition analysis of spatial relationships between monthly weather and air pollution index in China

Libo Zhang[1] · Yongqiang Liu[2] · Fengjun Zhao[2,3]

Published online: 30 November 2017

Abstract
Spatial patterns are important features for understanding regional air quality variability. Statistical analysis tools, such as empirical orthogonal function (EOF), have been extensively used to identify and classify spatial patterns. These tools, however, do not directly reveal the related weather conditions. This study used singular value decomposition (SVD) to identify spatial air pollution index (API) patterns related to meteorological conditions in China, one of world's regions facing catastrophic air pollution. The monthly API and four meteorological variables (precipitation, surface air temperature, humidity, and wind speed) during 2001–2012 in 42 cities in China were used. The two leading SVD spatial patterns display the API anomalies with the same sign across China and opposite signs between northern and southern China, respectively. The meteorological variables have different relationships with these patterns. For the first pattern, wind speed is the most important. The key regions, where the correlations between the API field and the wind speed's SVD time series are significant at the 99% confidence level, are found nationwide. Precipitation and air temperature are also important in the southern and northern portions of eastern China, respectively. For the second pattern, the key regions occur mainly in northern China for temperature and humidity and southern China for wind speed. Air humidity has the largest contribution to this pattern. The weather-API relationships characterized by these spatial patterns are useful for selecting factors for statistical air quality prediction models and determining the geographic regions with high prediction skills.

Keywords Statistical analysis · SVD · Air pollution index · Weather · China

1 Introduction

Large-scale air quality often displays certain spatial patterns over a period of time, characterized by gradients of air pollutant concentrations, local centers, and similarities or contrasts between different regions. The annual fine particulate matter $PM_{2.5}$ concentrations in the United States, for example, generally increase from about 2 $\mu g/m^3$ in the central to about 15 $\mu g/m^3$ in the eastern and western coastal regions with the centers in southern California, the Great Lakes, and the Gulf coast (Tai et al. 2010). The ozone concentrations in Europe generally increase from its northern and northwestern portions to the Mediterranean coast centered in northern Italy and southern France (Guerreiro et al. 2014).

Weather is one of the contributors to the spatial air quality patterns (Honoré et al. 2008; Kassomenos et al. 2008; Wang et al. 2013; Yang et al. 2016). Atmospheric processes such as droughts and heat waves can lead to severe air pollution events over a large region (Wang et al. 2010). The $PM_{2.5}$ center in the southern California described above is associated with the stagnation condition characterized by anticyclonic system, weak wind, no precipitation, and high temperature (Tai et al. 2010). Weather patterns were found to be related to the orientation, gradients, and characteristic patterns of daily air quality index

✉ Yongqiang Liu
yliu@fs.fed.us

[1] International Center for Ecology, Meteorology and Environment, College of Applied Meteorology, Nanjing University of Information Science and Technology, Nanjing 210044, China

[2] Center for Forest Disturbance Science, USDA Forest Service, 320, Green St, Athens, GA 30602, USA

[3] Research Institute of Forest Ecology, Environment and Protection, Chinese Academy of Forestry, 2 Dongxiaofu, Xiangshan Road, Beijing 100091, China

(AQI) in the northern Mid-Atlantic of the United States (Croft and Melendez 2009). Understanding the air quality spatial patterns and their weather relationships would help identify the major processes and mechanisms for the formation of air pollution events and develop prediction tools.

China is one of the world's regions where air pollution has escalated dramatically in the recent decades (UN 2001). In 2013, 70 out of 74 major cities in China failed to meet the ambient air quality standards for more than 144 days. In 2010, the high PM pollution was linked to 1.2 million premature deaths in China (Murray et al. 2012; WHO 2014). Like in the United States, Europe, and many other world regions, air pollution in China varies spatially (Li and Wang 2013; Wei et al. 2009; Li et al. 2013; Wang et al. 2013). The $PM_{2.5}$ concentrations in China increase from about 25 $\mu g/m^3$ in the southern coast to more than 60 $\mu g/m^3$ in northern China with a center of over 100 $\mu g/m^3$ in the Beijing mage-urban area (Rohdel and Muller 2015), and weather is an important factor for the regional variability of air quality in the most polluted regions in China (Kang et al. 2009; Han et al. 2009; Wang et al. 2010; Zhang et al. 2014).

A large number of efforts have been made to monitor air pollutions and analyze their relationships with weather. One of the monitoring efforts was to measure air pollutants and build an air pollution index (API) from 2000 in 42 key cities in China. The API data have been extensively used (Han et al. 2007; Li 2009; Liu et al. 2011; Li et al. 2012, 2013; Ren et al. 2013; Zhu et al. 2013; Zhan et al. 2013; Zhang et al. 2016; Tao et al. 2016). For example, Yu et al. (2011) described the multi-dimensional phase space for the API time series during a 10-year period in Lanzhou, northwestern China and found obvious chaotic characteristics resulted from the evolution of non-linear chaotic dynamic systems.

The research on the weather-air quality relationship in China as well as other world regions has been focused on daily scale. However, there is increasing attention to long-term (e.g., monthly and seasonal) relationships due to more frequent occurrences of persistent air pollution events such as forest and agricultural residue fires (Marlier et al. 2013), winter residence heating, and spring dust storms (Zhang et al. 2016). Long-term air pollution can affect outdoor activities such as construction, farming, recreation, and sport events.

Statistical techniques have been widely used to analyze spatial air quality patterns and their empirical relationships with weather (Cobourn 2007; Stadlober et al. 2008; Genc et al. 2010; Zhang et al. 2012; Chien and Bangdiwala 2012; Peterson et al. 2014; Gocheva-Ilieva et al. 2014; Kuo et al. 2015; Shahraiyni and Sodoudi 2016; Alyousifi et al. 2017). Statistical models have great potential for long-term air quality prediction through using averaged long-term meteorological conditions provided by operational weather forecasts. Also, statistical models are much more computationally efficient, which is critically important for operational long-term air quality prediction. In contrast, dynamical models (Wang et al. 2004; Byun and Schere 2006; Sofiev et al. 2006; Tian et al. 2016) need much larger computational resources to calculate complex atmospheric air pollutant dispersion and transport, mixing and deposition, and chemical reactions. In addition, dynamical models depend on initial atmospheric forcing, which can affect the subsequent atmospheric processes only for a short period. As a result, current real-time air quality prediction using dynamical models is mostly for 1–3 days (Zhang et al. 2012).

One problem with statistical techniques is that, despite air pollutants emitted mostly locally, air quality at a specific location could be strongly affected by remote conditions due to atmospheric transport. Different from dynamical models which explicitly simulate air pollutant transport and the related remote air quality effects of local pollutant emissions, statistical techniques such as correlation and regression analyses mostly consider the weather-air quality relationships at individual sites.

Some spatial analysis tools can help solve this problem to certain extent. Empirical orthogonal function (EOF), for example, has been used to separate air quality conditions into spatial patterns and temporal variations (Deng et al. 2013) through linear transformations of a field varying in both space and time. A small number of spatially orthonormal patterns are used to represent as much of the variance as possible. Singular value decomposition (SVD) (Bretherton et al. 1992; Wallace et al. 1992; Hu 1997; Wu and Wu 2010) has the same capacity as EOF, but it separates spatial patterns and temporal variations through linear transformations of two fields varying in both space and time and uses a small number of spatial patterns to represent as much of the covariance as possible. Thus, SVD is more powerful than EOF in understanding the interactions between two fields. Bretherton et al. (1992) compared several methods of spatial analyses and indicated that SVD is very simple to perform and interpret, has good general performance without systematic bias, and directly produces explicit measures of relationships between the derived coupled patterns. An extremely valuable application of SVD for predictive purposes can be obtained through analyzing the heterogeneous correlation map, defined as cross-correlations of a data field and its linear combination with the SVD expansion coefficient series of the other data field (Hu 1997).

SVD has been extensively used in meteorological research (Wallace et al. 1992; Ding and Jiang 1996; Zhang et al. 2010; Wang et al. 2011; Wang and Li 2012; Yao and Li 2013; Susan and Christopher 2014; Ma et al. 2015; Yao

et al. 2016). Wallace et al. (1992) compared applications of several spatial analysis techniques to the interannual coupling between wintertime Pacific sea surface temperature anomalies and atmosphere 500-mb height and found that SVD clearly isolates the two most important extratropical modes of variability. Liu (2003a and b) found that the prediction using the coupled SVD patterns are more skillful than using statistical relationships at individual sites. Tao et al. (2014) applied SVD to identify the relationships between local temperature and remote sea-surface temperature (SST) and found that extreme temperatures over the Poyang Lake Basin were closely related to the North Pacific SST. However, only few applications to ozone spatial patterns in tropical and South Korea regions (Kim et al. 2008; Seo et al. 2014) and environmental studies (Zekri et al. 2016) are found.

This study was to analyze the spatial patterns of the air quality index in China using the SVD technique. The questions to be answered included (1) what are the leading air pollution index spatial patterns that are closely related to meteorological conditions, (2) what are the key geographic regions where the weather-air quality index correlations are statistically significant, and (3) what are the dominant meteorological variables for each of the leading spatial air quality index patterns. The answers are expected to provide scientific evidence for developing statistical prediction tools for long-term air quality in China, as well as other world regions.

2 Methods

2.1 Research area

Air quality in China was investigated (Fig. 1). For the convenience of description, China is classified into seven administrative divisions: Northwest (NW), North (NC), Northeast (NE), East (EC), South (SC), Central (CC), and Southwest (SW) China. The following terms for geographic regions are also used: northern China (including NW, NC, and NE) and southern China (other divisions), western China (the NW and SW portions west of 100°E) and eastern China (rest of China), southeastern China (intersection of southern and eastern China), northeastern China (intersection of northern and eastern China), southwestern China (intersection of southern and western China), and northwestern China (intersection of northern and western China).

2.2 Air quality and meteorological data

The air pollution index (API) was used in this study. China began to measure PM_{10}, SO_2, NO_2, and other air pollutants in 2000 in 42 key cities of environmental protection (increased to 84 cities in 2004) by the Ministry of Environmental Protection of China (http://www.mep.gov.cn). API is estimated as follows. The concentration of each pollutant is simplified as a single conceptual index according to the pollutant concentration grading limit table. The pollutant whose individual air pollution index is the maximum among all kinds of pollutants is regarded as the primary pollutant and its individual air pollutant index is defined as the air pollution index. If the maximum individual air pollutant index is the same for two or more pollutants, the primary pollutant is selected according to the order of PM_{10}, SO_2, and NO_2. Daily API values were used to evaluate air pollution levels: 0–50 (excellent), 51–100 (good), 101–200, 201–300, and 301–500 (mild, moderate and severe pollution). We selected the API sites and years with complete records. Thus, the data from January 2001 to December 2012 at the first 42 sites (Fig. 1) were used for this study.

Daily meteorological variables of precipitation (P), air temperature (T), water vapor pressure (E), and wind speed (V) at the corresponding 42 weather stations were obtained from the China Meteorological Science Data Sharing Service Network (http://cdc.nmic.cn).

Each original daily series at a site/station was first converted to a monthly series, which consists of 144 samples (12 years × 12 months). The seasonal cycle was then filtered out by subtracting each value of a month from its multiple-year average. The new series was further normalized by dividing the standard deviation.

2.3 Singular value decomposition

Bretherton et al. (1992) applied the singular value decomposition (SVD) to pattern analysis of two data series. Here we briefly describe the SVD method following their notations and some terms used in Hu (1997). We denote the API data field as $s(x,t)$ and a meteorological variable as $z(x,t)$, where x is space location and t is time. The SVD analysis is a linear transformation:

$$s(x,t) \approx \sum_{n}^{N} a_n(t)p_n(x), \quad (1)$$

$$z(x,t) \approx \sum_{n}^{N} b_n(t)q_n(x), \quad (2)$$

that identifies pairs of coupled spatial patterns, $p_n(x)$ and $q_n(x)$ (also called left and right SVD spatial patterns, respectively), and their temporal expansion coefficients, $a_n(t)$ and $b_n(t)$. Here N is the number of SVD modes, which is equal to the number of space locations. The SVD

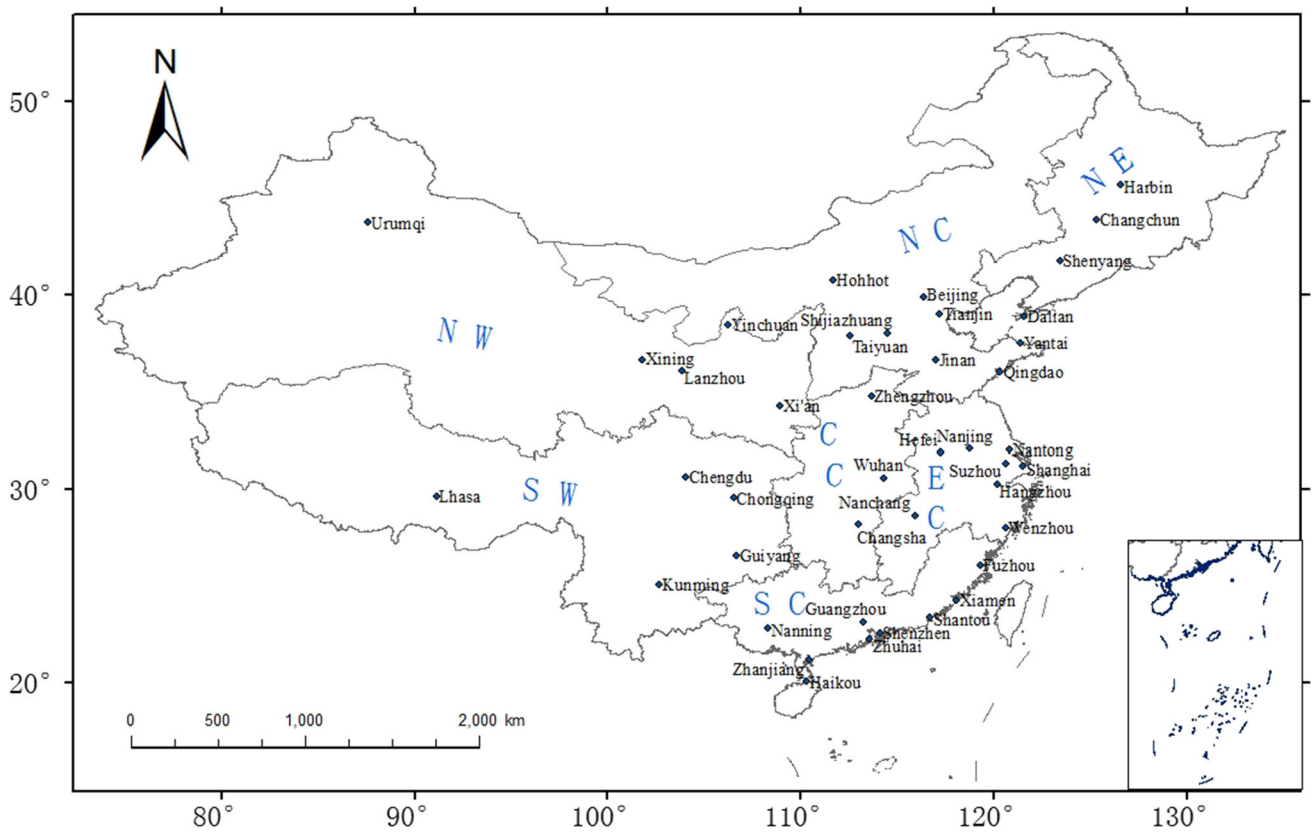

Fig. 1 The air quality measurement sites. Also shown are the administrative divisions of Northwest (NW), North (NC), Northeast (NE), East (EC), South (SC), Central (CC), and Southwest (SW) China

analysis was conducted as follows: First, the cross-covariance matrix of $s(x, t)$ and $z(x, t)$, C_{sz}, was calculated. Secondly, the eigenvalues (also called singular values) σ_n of the matrix were obtained by solving $|C_{sz} - \sigma I| = 0$ where I is the Identity matrix. Next, the eigenvectors [that is, the SVD patterns $p_n(x)$ and $q_n(x)$] corresponding to each eigenvalue were obtained. $p_n(x)$ and $q_n(x)$ and $a_n(t)$ and $b_n(t)$ are the components of an SVD mode.

All modes are arranged so that their σ_n appear in descending order (i.e., $\sigma_i \geq \sigma_j$ if $i<j$). The first pair of singular patterns describes the largest fraction of the squire covariance between the two fields and each succeeding pair describes a maximum fraction of square covariance that is unexplained by the previous pairs. The contribution of the nth mode to the total covariance of the two fields is measured by squared covariance fraction.

$$SCF_n = \sigma_n^2 / \sum_n^N \sigma_n^2, \tag{3}$$

and the cumulative contribution from the first k modes, $CSCF_n$, is the sum of their SCF_n. The variance contributions of $p_n(x)$ to $s(x, t)$ and $q_n(x)$ to $z(x, t)$ are defined as

$$C_{n,p} = \sum_t^K a_n^2(t) / \sum_n^N \sum_{t=1}^K s(n, t), \tag{4}$$

$$C_{n,q} = \sum_t^K b_n^2(t) / \sum_n^N \sum_{t=1}^K z(n, t), \tag{5}$$

The correlations between expansion coefficient series

$$r_n \approx \sum_t^K a_n(t) b_n(t), \tag{6}$$

have the feature with their magnitude that $r_i \geq r_j$ if $i<j$. The heterogeneous correlation maps are defined as:

$$cor_{left,n} \approx \sum_t^K s(x,t) b_n(t), \tag{7}$$

$$cor_{right,n} \approx \sum_t^K z(x,t) a_n(t), \tag{8}$$

They are called left and right heterogeneous correlations, respectively. The SVD analysis would produce $cor_{left,n}(x)$ from Eq. 7 and $q_n(x)$ from Eq. 2 based on historical measurements. If $z(x, t + 1)$ is known from prediction (e.g., weather forecast), $b_n(t+1)$ can be obtained from

Eq. 2. Then *s(x, t + 1)* (future API) can be obtained from Eq. 7.

The SVD analysis was conducted using NCL (https://www.ncl.ucar.edu/) and MATLAB (https://www.mathworks.com/product/ltc/matlab.html). Same results were obtained from the two tools.

2.4 Analysis method

SVD analysis was made separately between API and *P*, *T*, *E*, or *V*. The SVD analysis of this study was focused on left heterogeneous correlations, $cor_{left,n}(x)$, because the purpose of this study was to provide scientific evidence for developing statistical prediction tools for long-term air quality index [that is, *s(x,t)*] based on meteorological conditions [that is, $b_n(t)$]. The areas where the correlations were statistically significant at the 99% confidence level ($p < 0.01$ and the critical value is 0.22) were defined as key regions. The correlations within the key regions that were significant at the 99.9% level ($p < 0.001$ and the critical value is 0.28) were regarded as strongly significant. The correlations in other regions that were significant at the 95% level ($p < 0.05$ and the critical value is 0.17) were regarded as weakly significant.

3 Results

3.1 API spatial patterns and temporal variations

Annual API is larger in northern than southern China, increasing from about 40 in SC to over 100 in Lanzhou and Urumqi of NW. API is larger in winter (Fig. 2; Table 1), 176 in Urumqi and 145 in Lanzhou. In spring, the API center at Urumqi no longer exists, while API at Lanzhou is reduced to 128. API is the lowest in summer, only about 80 in NW and NC. API bounces back to about 90 in autumn, with Urumqi becoming a pollution center again. Coal combustion and dust are the major air pollution sources in China, whose emissions are the largest during winter and spring, respectively (Li et al. 2012). Weather is dry and windy with frequent temperature inversion during the two seasons, leading to more severe pollutant conditions.

Annual and seasonal APIs averaged over China decreased during the 2001–2012 period (Fig. 3). The largest decrease occurred in springs during the first 3 years. Among the three API components, PM_{10} was a dominant contributor (about 80% during winter, and 90–95% during other seasons) (Li et al. 2012). PM_{10} declined remarkably over the years, same as API, mainly due to decreasing wind speed and increasing precipitation in NW, while SO_2, and NO_2 either had no clear trends or declined slightly after 2007.

Note that this trend differs from the fact that the air quality in China has been worsening in the recent decade, mainly caused by dramatic increases in man-made air pollutant emissions (sulfates, nitrates, etc.) due to the rapid increases in industry size, automobile number, and urbanization. While some particles such as biomass smoke could occur at both fine (2.5 μm or smaller in dynamic diameter) and coarse (> 2.5 μm) scales and therefore their PM_{10} concentrations are often proportional to $PM_{2.5}$ concentrations, the man-made air pollution particles are mainly at fine scales and most natural air pollution particles such as dust, sea-salt, etc. are mainly at coarse scales. Thus, API, which includes PM_{10} but not $PM_{2.5}$, mainly reflects the recent trend in concentrations of natural air pollutants.

3.2 Leading SVD modes

The squared covariance fraction of the first SVD mode (SCF_1) is greater than 50% for all meteorological variables (Table 2). The accumulated *SCF* are greater than 80% for the first two modes ($CSCF_2$) except for precipitation, which is 70%. SCF_3, however, is reduced to a single digit. Thus, only the first two SVD modes are analyzed below.

3.3 SVD patterns and time series

In the description below, we will simply denote SVD heterogeneous correlations between API and a meteorological variable $MET = P,\ T,\ E,$ or V as $cor_{l,n}(MET)$, where $l =$ left or right and n is mode; the SVD expansion coefficients as $a_n(MET), b_n(MET)$; and the correlations between the coefficient series as $cor_{l,n}(MET)$.

3.3.1 Precipitation

$cor_{left,1}(P)$ (Fig. 4a) is positive across China except for a small SW area with extensive key regions over southeastern China. The correlations in most of the key regions are strongly significant. In addition, the correlations in NC are weakly significant. Correlations in other regions are insignificant. $cor_{right,1}(P)$ (Fig. 4b) is mostly negative in eastern China with a small key region along the southeastern coast. This result indicates that lower precipitation will result in higher air pollution index in eastern China and the role of precipitation is important for air quality mainly in southeastern China.

Note the sign ambiguity with SVD analysis (Bro and Kolda 2008). The cross-covariance matrix of *s(x, t)* and *z(x, t)* would yield a pair of *p(x)* and *q(x)* with *a(t)* and *b(t)*, or a pair of $-\ p(x)$ and $-\ q(x)$ with $-\ a(t)$ and $-\ b(t)$. The negative pair would yield the same left and right heterogeneous correlations shown in Fig. 4a and b but with

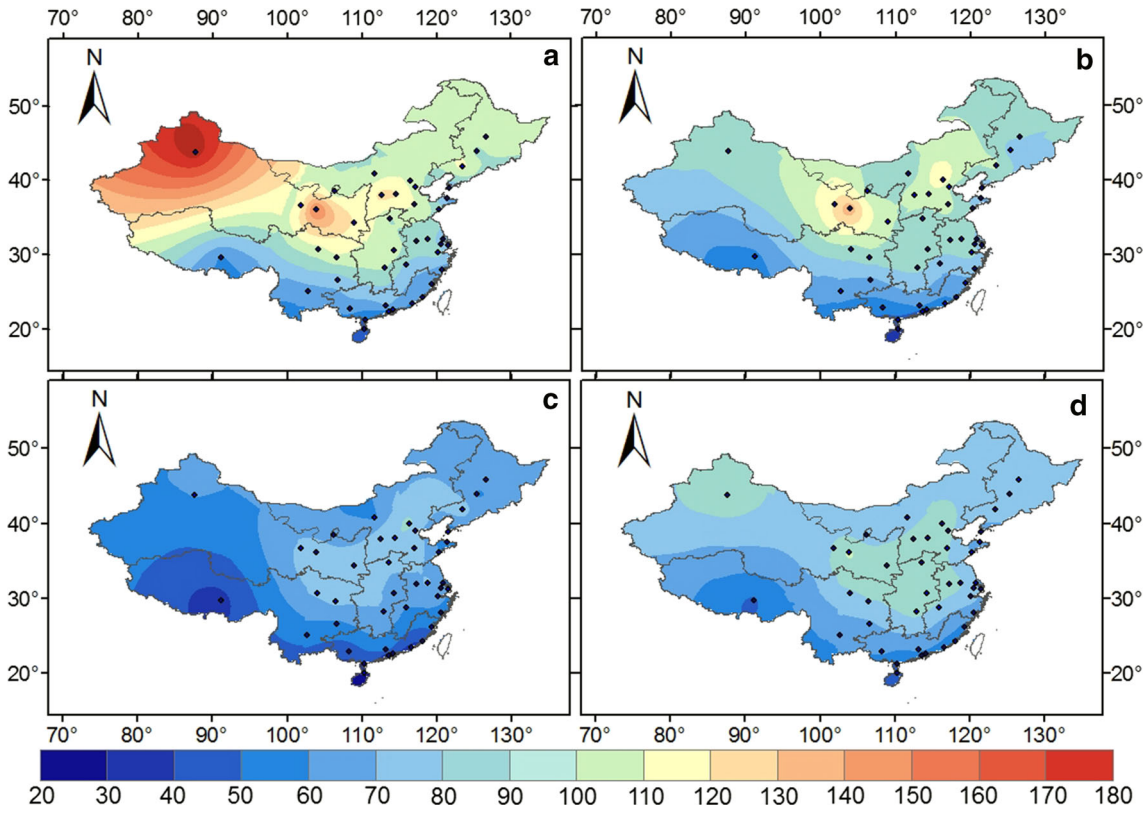

Fig. 2 Spatial API distributions during winter, spring, summer, and autumn (**a**–**d**). The dots are measurement sites

Table 1 Monthly API values averaged 2001–2012 in 7 divisions and entire China

Season	NW	NC	NE	EC	SC	CC	SW	China
Winter	125.4	95.3	90.1	77.7	58.4	91.8	78.5	88.2
Spring	100.8	89.6	80.7	79.7	53.2	85.2	72.2	80.2
Summer	70.1	70.4	63.4	62.8	40.7	69.2	58.6	62.2
Autumn	85.0	78.8	72.0	74.3	54.7	85.1	66.5	73.8
Annual	95.3	83.5	76.6	73.6	51.8	82.8	69.0	76.1

NW, NC, NE, EC, SC, CC, and SW represent Northwest, North, Northeast, East, South, Central, and Southwest China (see Fig. 1 for the seven administrative divisions in China)

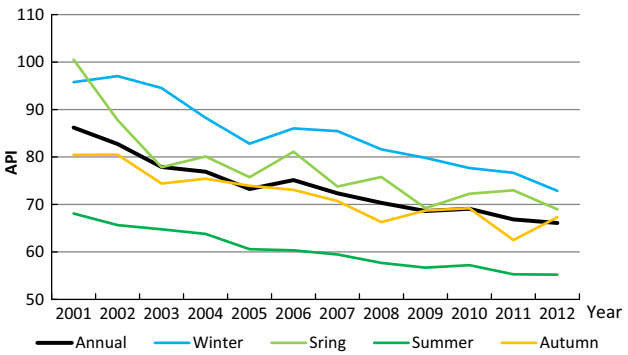

Fig. 3 Inter-annual variations of annual and seasonal API values averaged over 42 sites in China

opposite signs. This means that more precipitation will result in lower air pollution.

$cor_{left,2}(P)$ (Fig. 4c) is negative in southeastern China and positive in other regions. No key region is found despite weakly significant correlations in NE and NC as well as a very small western SW area.$cor_{right,2}(P)$ (Fig. 4d) is mostly negative in northeastern China and positive in southeastern China, also without a key region. Thus, API and precipitation change oppositely, which is the same as mode 1. The differences are that, instead of the same sign across eastern China, the changes in API or precipitation are opposite between its southern and northern portions, and the relationship is not close without key regions.

The accumulated variance contribution of the first two API modes to the original API field is 42.27%. The corresponding contribution for precipitation, however, is only 14.86% (Table 2), suggesting that even a small precipitation anomaly could lead to a large change in API.

$A_n(P)$ and $b_n(P)$ (n = 1, 2) tend to decrease over the analysis period (Fig. 5). The magnitude of the decline is larger for API than precipitation. Their short-term (inter-

Table 2 Singular values (σ), squared covariance fraction (*SCF*), cumulative squared covariance (*CSCF*),contribution of left (right) SVD pattern to the variance of left (right) field, C_{API} (C_{MET}), and correlation between the left and right SVD time coefficient series *r*. *P*, *T*, *E*, and *V* represent precipitation, temperature, water vapor pressure, and wind speed, respectively

Met	Mode	σ	SCF (%)	CSCF (%)	C_{API} (%)	C_{MET} (%)	*r* (%)
P	1	3.41	57.80	57.80	27.9	8.28	0.54
	2	1.61	12.80	70.60	14.37	6.58	0.40
	3	1.11	6.08	76.68	3.58	8.27	0.49
	4	1.04	5.36	82.04	4.85	4.55	0.53
T	1	7.14	80.63	80.63	30.52	52.42	0.43
	2	2.68	11.38	92.00	9.89	11.62	0.60
	3	1.38	3.02	95.02	5.01	8.26	0.51
	4	0.95	1.44	96.46	4.82	4.90	0.47
E	1	5.69	68.84	68.84	21.58	35.42	0.49
	2	2.58	14.16	83.00	20.93	7.20	0.50
	3	1.61	5.48	88.48	6.13	7.23	0.58
	4	1.33	3.78	92.26	3.89	7.41	0.60
V	1	11.26	87.08	87.08	32.73	30.72	0.85
	2	2.69	4.97	92.05	8.39	9.33	0.73
	3	2.02	2.79	94.85	8.70	5.96	0.67
	4	1.48	1.49	96.34	5.53	4.54	0.71

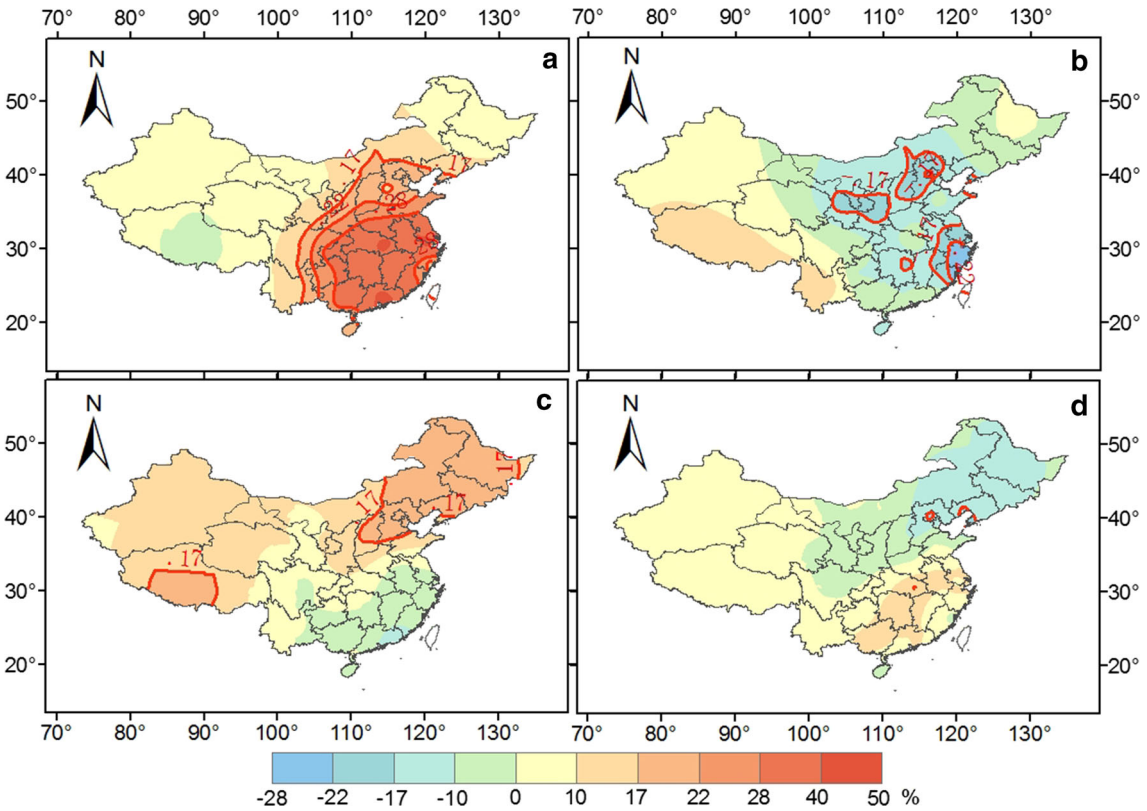

Fig. 4 Spatial patterns of heterogeneous correlations between API and precipitation: left and right correlations of mode 1(**a**–**b**) and mode 2 (**c**–**d**)

monthly) variations have the same signs except for a number of time segments (e.g., the first half of 2001, 2008 and 2011 for mode 1). $r_n(P)$is 0.54 (n = 1) and 0.4 (n = 2) ($p < 0.001$ for both) (Table 2). The magnitude of the short-term variations is also larger for API than precipitation for each mode.

The long-term (inter-annual) decline trend can be interpreted as follows. For n = 1, for example,$cor_{left,1}(P)$ is determined by the product of *API* and $b_1(P)$ (Eq. 7). API

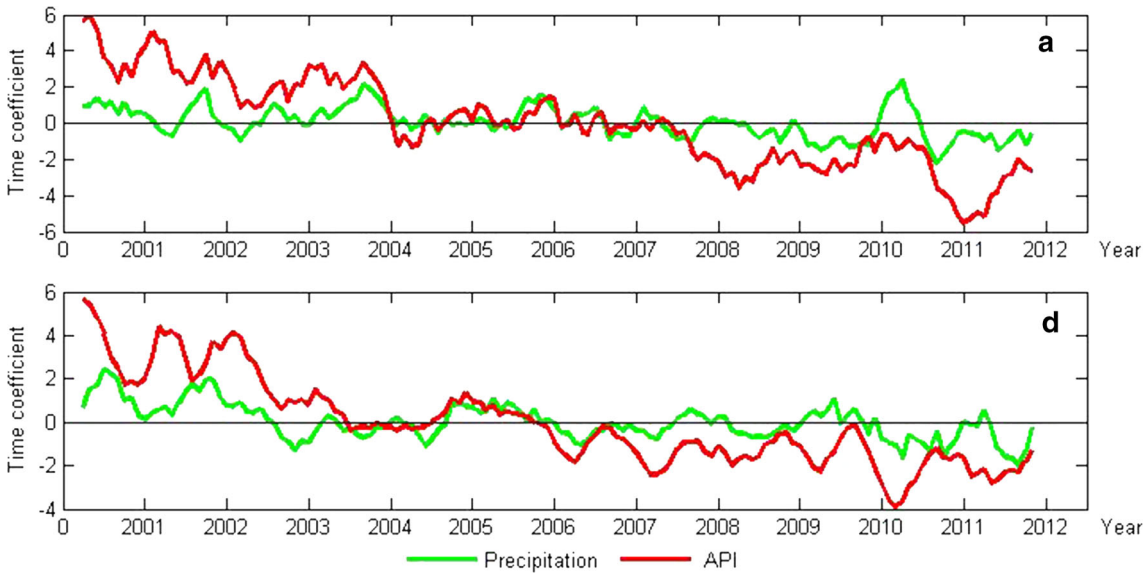

Fig. 5 SVD time coefficient series between API and precipitation for modes 1 (**a**) and 2 (**b**)

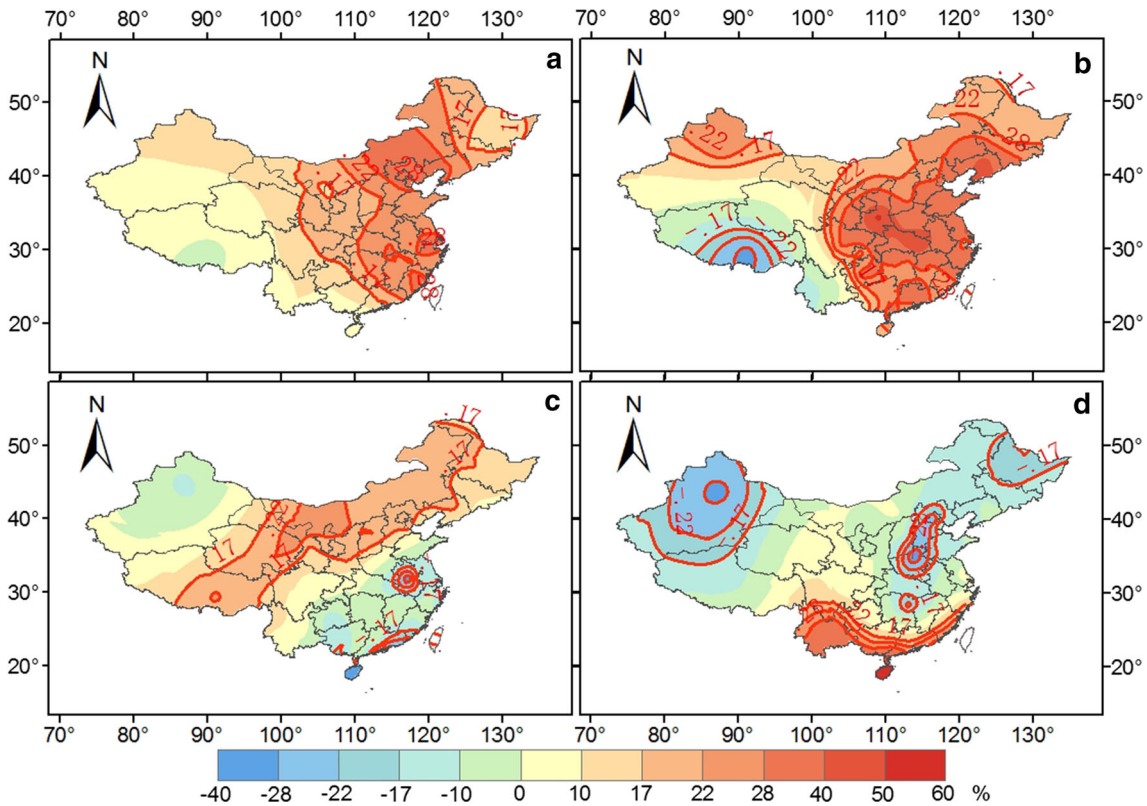

Fig. 6 Spatial patterns of heterogeneous correlations between API and air temperature: left and right correlations of mode 1(**a**–**b**) and mode 2 (**c**–**d**)

declines over the analysis period (Fig. 3), meaning that the normalized API is positive in the first portion of the period and negative in the second portion. Because $cor_{left,1}(P)$ is positive (Fig. 4a), $b_1(P)$ has to be positive in the first portion and negative in the second portion.

3.3.2 Air temperature

Similar to $cor_{left,1}(P)$, $cor_{left,1}(T)$ (Fig. 6a) is positive across China with the key regions in eastern China. The correlations in NC are strongly significant. In addition, the

correlations in NE and eastern NW are weakly significant. $cor_{right,1}(T)$ (Fig. 6b) is positive in eastern China with extensive key regions. Correlations in the key regions are mostly strongly significant. The sign is opposite to $cor_{right,1}(P)$, meaning higher surface air temperature will result in higher air pollution index in this region. In addition, positive and negative correlations with small areas of key regions are found in the western NW and SW, respectively, but the corresponding $cor_{left,1}(T)$ is very small in these regions.

Also similar to $cor_{left,2}(P)$, $cor_{left,2}(T)$ (Fig. 6c) is positive with a small area of key regions in the western NC and eastern NW. The correlations in the two sides of the key region from western SW to NE, however, are weakly significant. Meanwhile, $cor_{left,2}(T)$ is negative in southeastern China with the key regions at a few sites. $cor_{right,2}(T)$ (Fig. 6d) is positive and negative in NW and most eastern China with the key regions in a narrow southern coastal zone, NC, and NW. Unlike mode 1, however, there is no corresponding close relationship between $cor_{left,2}(T)$ and $cor_{right,2}(T)$.

The long-term trends and short-term variations with $a_n(T)$ and $b_n(T)$ (n = 1, 2) (Fig. 7) are similar to those of precipitation. The difference is that the magnitude of short-term variations is comparable between API and temperature, except at a few times when the magnitude of temperature short-term variations is larger. $r_n(T)$is 0.43 (n = 1) and 0.6 (n = 2) ($p < 0.001$ for both) (Table 2).

3.3.3 Water vapor pressure

$cor_{left,1}(E)$ (Fig. 8a) is positive with the key regions in eastern NW, NC, and NE (strongly significant in NC), and negative in southeastern China without a key region. $cor_{right,1}(E)$ (Fig. 8b) is mostly positive except for NE, with the key regions (mostly strongly significant) in western and southeastern China. $cor_{left,2}(E)$ (Fig. 8c) is positive across China with the key regions (mostly strongly significant) in southeastern China. $cor_{right,2}(E)$ (Fig. 8d) is negative in eastern China with a small area of key region in western NW, but positive with the key regions in western China.

The spatial patterns of mode 1 (2) for water vapor pressure are similar to those of mode 2 (1) for precipitation. Thus, water vapor pressure has the same role as precipitation in air pollution anomalies described above. The difference is that water vapor pressure is a more important meteorological variable for the opposite air quality index anomalies between southern and northern China, while precipitation is more important for the same air quality change across eastern China. In addition, the magnitude of the positive values in $cor_{left,1}(E)$ (Fig. 8a) and $cor_{right,1}(E)$(Fig. 8b) is much larger than the corresponding values in $cor_{left,2}(P)$ (Fig. 4c) and $cor_{right,2}(P)$(Fig. 4d), while the key regions are located mainly in western China for $cor_{right,2}(E)$(Fig. 8d) rather than eastern China for $cor_{right,1}(P)$ (Fig. 4b).

The long-term trends and short-term variations with $a_n(E)$ and $b_n(E)$ (n = 1, 2) (Fig. 9) are similar to those of precipitation. $r_n(E)$is 0.49 (n = 1) and 0.5 (n = 2) ($p < 0.001$ for both) (Table 2).

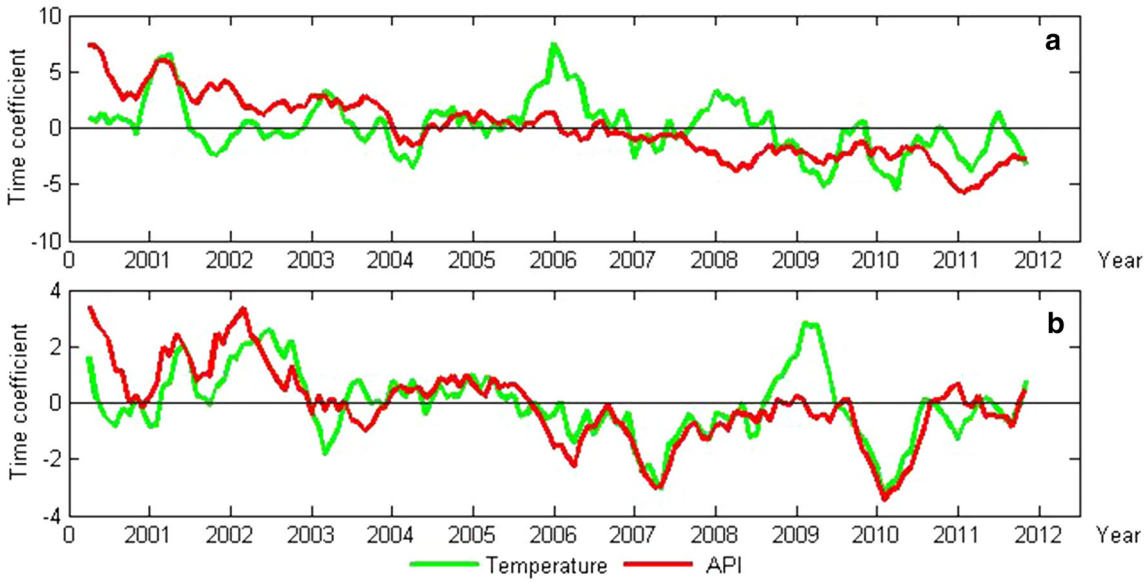

Fig. 7 SVD time coefficient series between API and air temperature for modes 1 (**a**) and 2 (**b**)

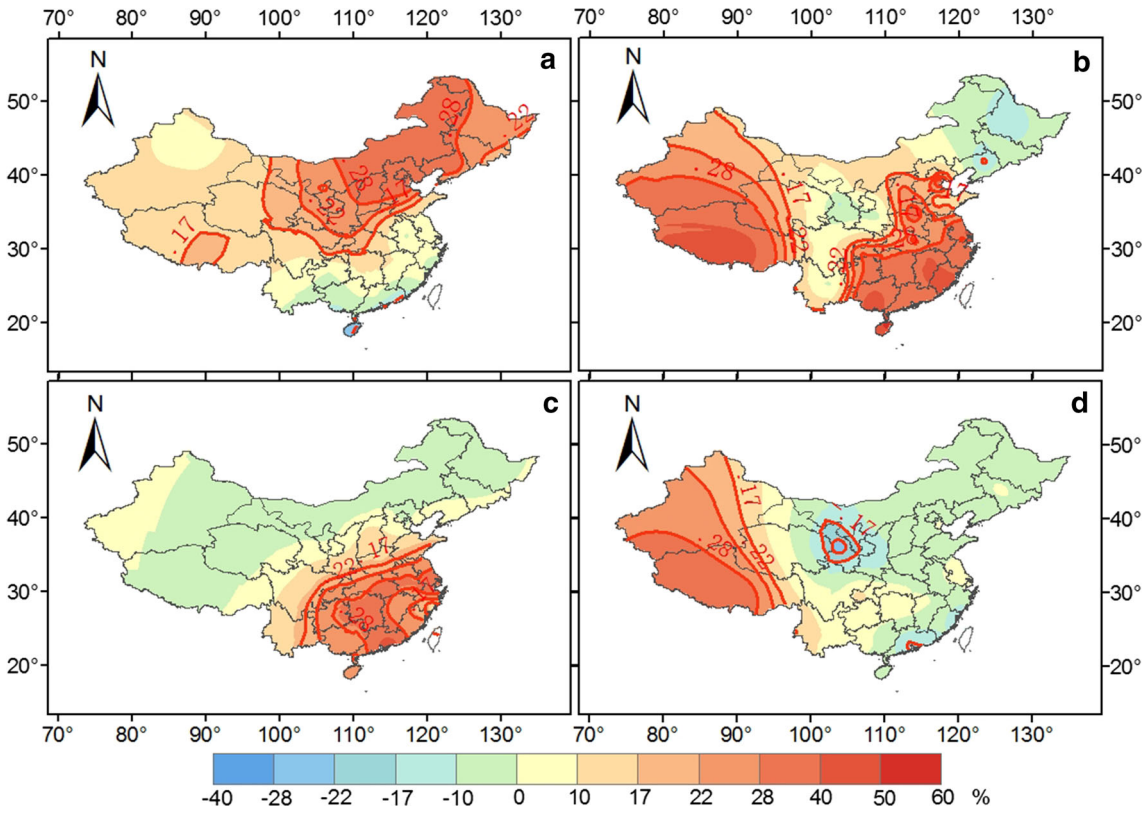

Fig. 8 Spatial patterns of heterogeneous correlations between API and water vapor pressure: left and right correlations of mode 1(**a**–**b**) and mode 2 (**c**–**d**)

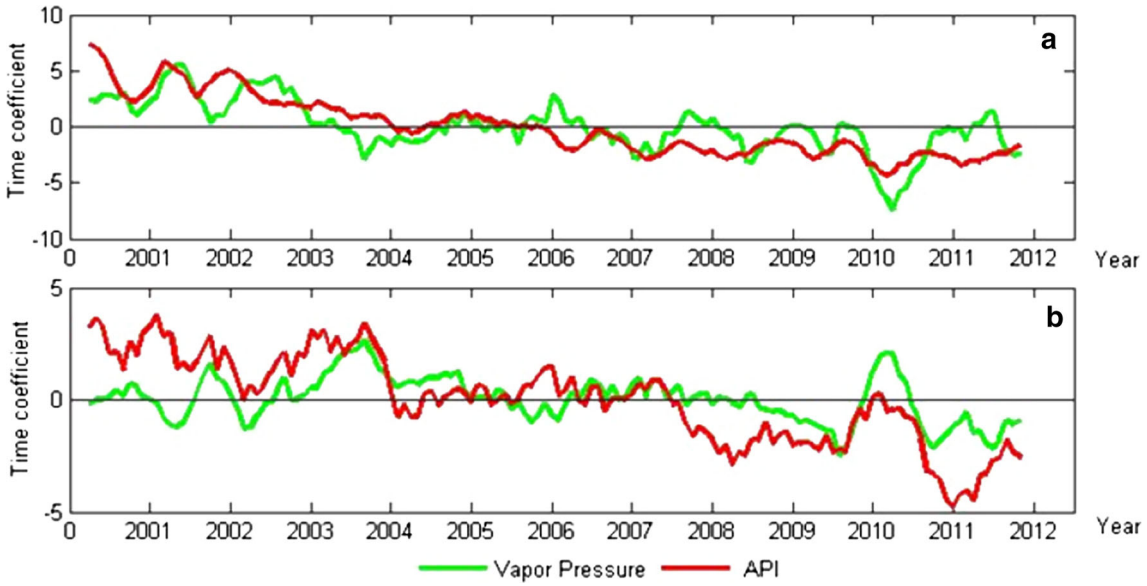

Fig. 9 SVD time coefficient series between API and water vapor pressure for modes 1 (**a**) and 2 (**b**)

3.3.4 Wind speed

$cor_{left,1}(V)$ (Fig. 10a) is positive with the key regions covering all of China. The correlations are strongly significant everywhere except a small area along the southern coast. The values even reach 0.5 in NC. $cor_{right,1}(V)$ (Fig. 10b) is positive with the key regions in NC and NE as well as a small area of NW, and negative in SC and eastern SW without a key region. Thus, stronger winds in northern

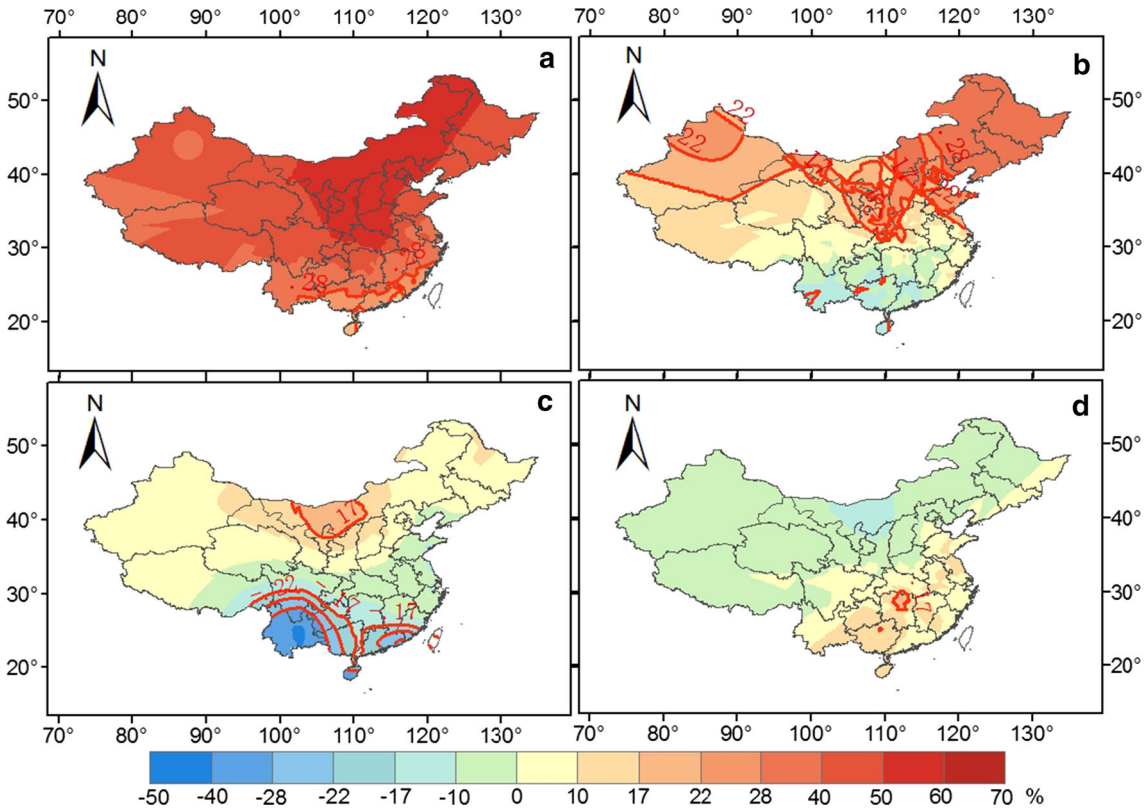

Fig. 10 Spatial patterns of heterogeneous correlations between API and wind speed: left and right correlations of mode 1(**a**–**b**) and mode 2 (**c**–**d**)

China and weaker winds in southern China lead to larger air pollution index.

$cor_{left,2}(V)$ (Fig. 10c) is negative in southern China with the key regions along the southern coast, and positive in northern China with weakly significant correlations in northern NC. The $cor_{right,2}(V)$ (Fig. 10d) is positive in southern China and negative in northern China without a key region. The spatial patterns indicate that stronger wind lead to lower air pollution index in both southern and northern China.

$a_1(V)$ and $b_1(V)$ (Fig. 11) decline remarkably with time. $a_2(V)$ and $b_2(V)$ however have a totally different long-term trend, decreasing from 2001 to 2003, staying low until 2007, and then increasing towards 2012. Their short-term variations for both modes are relatively smaller. $r_n(V)$ is 0.85 (n = 1) and 0.73 (n = 2) ($p < 0.001$) (Table 2), both the highest among the four meteorological variables.

4 Discussion

4.1 Spatial air pollution index patterns

With a 50–80% contribution to the total covariance of API and wind, precipitation, or temperature, the same API anomalies across the entire eastern China (first SVD API pattern) should be mostly seen if the anomalies are driven by one or more of these meteorological variables. In contrast, with a 70% contribution to the total covariance of API and air humidity, the southern and northern portions of eastern China would more likely experience opposite API anomalies (the second spatial API pattern) if air humidity is a main weather driver.

There are several possible causes for the second pattern of regional differences mainly between the south and north rather than the west and east. First, according to China's regulations, the government sponsored winter residence heating system with coal combustion as a major heat source in the past is operated in northern China rather than the entire country. Secondly, spring dust storms mainly have the tracks from west to east in northern China, while southern China is barely affected. Thirdly, the summer and winter monsoon systems in eastern China move in the south-north direction and often lead to opposite anomalies between the south and north. For example, a longer stay than normal in the south of the summer monsoon system would produce more rainfall there but less in the north, reducing API in the south while increasing it in the north.

4.2 Weather relationships

The weather conditions corresponding to the air pollution index anomalies cross entire eastern China (first pattern) are found to be lower precipitation/humidity, and higher

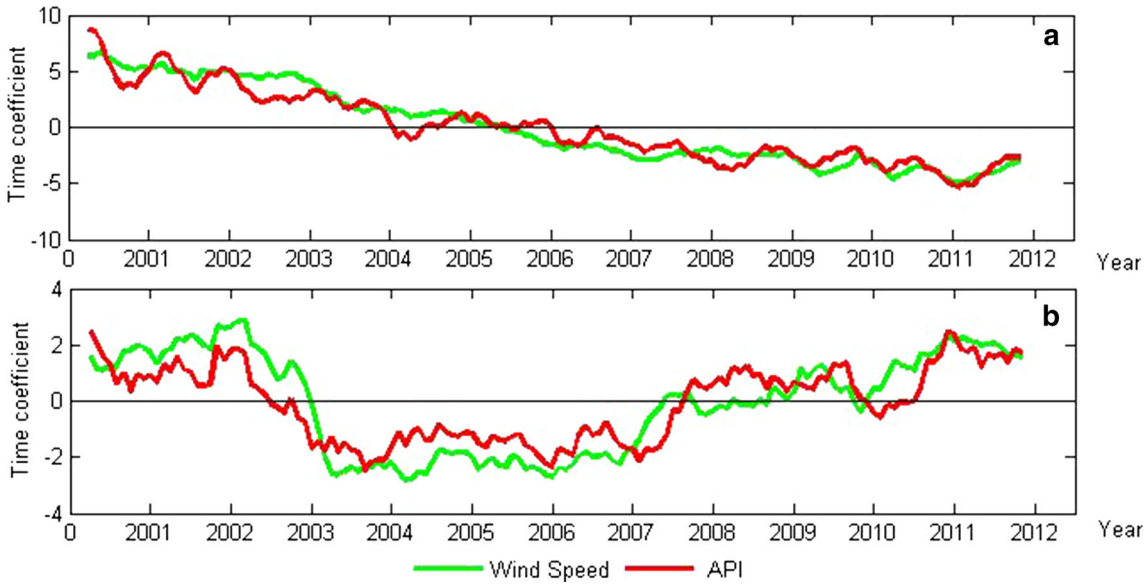

Fig. 11 SVD time coefficient series between API and wind speed for modes 1 (**a**) and 2 (**b**)

temperature in this region, and stronger wind speed in the northern and weaker in the southern portion. This agrees with the previous studies using other analysis approaches (Duan et al. 2008; Li 2009; Li et al. 2012, 2013; Deng et al. 2013). Rainfall and atmospheric water vapor can wash out air pollutants through wet deposition. Sands from dust storms and urban construction sites are one of the major PM_{10} sources in northern China. High wind speed and warm temperature lift more dust particles from the ground into the air in northern China, while larger wind leads to larger transport and dispersion from highly air polluted urban to less polluted rural area in southern China (Tian et al. 2005; Ren et al. 2005; Han et al. 2007; Li et al. 2014). This study further indicates that wind speed has the closest relationship with air pollution index and its impacts cover all of China for this pattern. The largest impacts occur in northeastern China for wind speed and air temperature, but in southeastern China for precipitation.

For the opposite air pollution index anomalies between southern and northern portions of eastern China (the second pattern), precipitation and humidity play the same role in air pollution index changes as the first pattern (that is, the larger they are, the less serious air pollution is). Humidity has the closest relationship with air pollution index among all variables for this pattern. Wind speed has the role as the first pattern in the southeastern China (that is, the larger wind speed is, the weaker air pollution index is). Temperature, however, plays an opposite role to the first pattern, that is, air pollution index becomes more serious in either northern or southern portion of eastern China when temperature is lower. High air temperature usually indicates unstable atmosphere, which is in favor of vertical transport of air pollutants.

4.3 Air pollution index prediction

The contributions of the first two SVD patterns to the variance of original API are about 40–42% (Table 2), suggesting that nearly half of the monthly API variations in China could be explained by meteorological variations. Thus, meteorological conditions could be useful for predicting API at monthly scale. The following procedure could be used to develop a prediction model. First, for one of the meteorological variables analyzed in this research [$z(x, t)$ in Eq. 2], its value at the next month, $t + 1$, can be obtained from operational monthly weather forecast provided by the weather services in many countries including China. Secondly, obtain time coefficient $b_n(t + 1)$ using $z(x, t + 1)$ and the SVD pattern, $q_n(x)$, which is already known from this study. Third, obtain the left field $s(x, t + 1)$ [i.e., $API(x, t + 1)$] using Eq. 7 based on $b_n(t + 1)$ and the left heterogeneous correlation, $cor_{left, n}(x)$, which is already known.

Note that the SVD formulas of Eqs. 2 and 7 are concurrent rather than predictive relationships. The prediction here is meant to use predicted weather for the next month to obtain the air pollution index of that month. Apparently, the skill of the prediction of monthly air pollution index is dependent on the skill of monthly weather prediction.

4.4 Air quality measurement sites

All API sites except two were located in eastern China (approximately east of 100°E). Thus, eastern China was fully represented, but geographical details in western China likely were missed in the SVD analysis.

Most sites were located in province capitals, with both administrative and scientific reasons. In China, major administration agencies of a province, including environmental protection and meteorological services, are located in the capital. Meanwhile, the capital usually is the largest city in the province with the largest population and industry and therefore is the most polluted. Thus, the air quality measurement sites were located mostly in the province capitals rather than being evenly distributed in space. However, in west of proximately 100°E, there are only two provinces of Xizhang (Tibet) and Xingjiang, so only two sites were found. The two provinces were sparsely populated and pollution was much less concerned in comparison with eastern China. Furthermore, many environmental factors such as industry category, population density, and topographic factors in addition to air pollutant emissions and weather can influence API in the sample cities. These factors need to be considered if simulating and predicting air pollution concentrations. But this is not the case for this study because it used the API measurements rather than modeling. The measurements already included the influences of all factors at providence level.

4.5 Conversion from site to grid-point values

The inverse distance weighting (IDW) method (Li and Heap 2008) was used to convert the API and the SVD results at the 42 sites to the regularly distributed grid points for plotting purpose. The IDW obtains the value of a grid point using the values at several nearby sites weighted by an inverse function of the distance between the grid point and each site based on the assumption that a site closer to the grid point is more similar to it than those sites further away in their values. The IDW works well for large-scale meteorological data (Nalder and Wein 1998). However, unlike the geostatistical technique such as the Kriging method, the IDW method does not consider the impacts of other factors with particular spatial structure such as topography, rural emission sources such as desert dust and farming-land biomass burning, etc. The data for these factors were unavailable for this study. Note that these limitations would not affect this study. First, as indicated above, the method was used to convert data from sites to grids for plotting purpose rather than to obtain more detailed values between sites. Secondly, as showed in the result section below, this study only analyzed two leading SVD patterns, first having the same sign and the second having opposite signs across China. They were large-scale patterns and the original data provided enough spatial resolution to represent these patterns.

5 Conclusions

The singular value decomposition (SVD) has been applied to identify the spatial air pollution index patterns in China and their weather drivers. The findings provide the answers to the three questions for this study. First, there are two leading patterns that are characterized by the same air pollution index anomalies across China and opposite anomalies between northern and southern China, respectively. Secondly, the key regions in the first pattern are nationwide in the correlations between the air pollution index filed and SVD time series of wind speed, southeastern China for the meteorological conditions of precipitation and humidity, and northeastern China for temperature. The key regions in the second pattern occur mainly in northern China for temperature and humidity and southern China for wind speed. Thirdly, the most important meteorological variables are wind speed for the first pattern, especially in the northern China, and air humidity for the second pattern. Wind speed and temperature may play opposite roles in air pollution index anomalies, depending on geographic regions and spatial patterns. It can be concluded that the long-term spatial patterns of air pollution index in China are closely related to weather conditions with the relationships varying with individual meteorological variables and geographic regions. These relationships could help develop statistical air pollution index prediction tools such as regression models by selecting appropriate prediction factors and expecting the locations with certain prediction skills.

API mainly considers PM_{10} concentration. China started to monitor $PM_{2.5}$, O_3 and CO in 2012, which together with the air pollutants included in calculating API are used to formulate AQI (Wang et al. 2014a, b). AQI is a better measure than API because $PM_{2.5}$ and O_3 are more closely related to air pollution events, such as smog and haze, and they have been increasing due to increasing auto numbers and other fine particulate emission, which is opposite to the long-term PM_{10} trend. AQI was not used in this study because of its short time series. However, it could be a good resource for future research.

Besides the ground measurements, the meteorological conditions in the planetary boundary layer (PBL) and free atmosphere such as PBL height and thermal stability are also important for air pollution (Han et al. 2009). These factors were not examined in this study. The physical mechanisms for the weather-air quality relationships need to be investigated through analyses of observational data and simulations with numerical models.

This study focused on the effects of meteorological fields on air pollution index. As atmospheric aerosols, air pollutants can affect the atmospheric radiation, clouds, and

local and regional climate (Liu 2005; Liu et al. 2013; Shi et al. 2014). Further research based on the coupled SVD weather-air quality patterns should be valuable to improving our understanding to the roles of air pollutants in regional climate anomalies.

Acknowledgements The air pollution index (API) data were obtained from the Ministry of Environmental Protection of China. The meteorological data were obtained from China Meteorological Science Data Sharing Service network. We would like to thank three reviewers and the Associate Editor for their valuable comments and suggestions. This study was supported by the China Natural Science Foundation under project 31670661 and USDA Forest Service.

References

Alyousifi Y, Masseran N, Ibrahim K (2017) Modeling the stochastic dependence of air pollution index data. Stoch Environ Res Risk Assess. https://doi.org/10.1007/s00477-017-1443-7

Bretherton CS, Smith C, Wallace JM (1992) An intercomparison of methods for finding coupled patterns in climate data. J Clim 5:541–560

Bro ER, Kolda T (2008) Resolving the sign ambiguity in the singular value decomposition. J Chemom 22:135–140

Byun DW, Schere KL (2006) Review of the governing equations, computational algorithms, and other components of the models-3 community multiscale air quality (CMAQ) modeling system. Appl Mech Rev 59:51–77

Chien LC, Bangdiwala SI (2012) The implementation of Bayesian structural additive regression models in multi-city time series air pollution and human health studies. Stoch Environ Res Risk Assess 26:1041–1051. https://doi.org/10.1007/s00477-012-0562-4

Cobourn WG (2007) Accuracy and reliability of an automated air quality forecast system for ozone in seven Kentucky metropolitan areas. Atmos Environ 41:5863–5875. https://doi.org/10.1016/j.atmosenv.2007.03.024

Croft PJ, Melendez BV (2009) Investigation of the air quality index as related to weather regime. Natl Weather Dig 33:132–153

Deng XJ, Liao LQ, Hu GP (2013) Air pollution index and their correlation with meteorological data in major cities of China during the last decades. Environ Sci Tech 36:70–75

Ding YG, Jiang ZH (1996) Generality of singular value decomposition in diagnostic analysis of meteorological field. Acta Meteorol Sin 54:365–372

Duan YS, Wei HP, Fu QY, Gao S, Huang R, Huang YM (2008) Regional spatio-temporal mode differences of air pollution index of key environmental protection cities in China. Acta Sci Circumstantiae 28:384–391

Genc DD, Yesilyurt C, Tuncel G (2010) Air pollution forecasting in Ankara, Turkey using air pollution index and its relation to assimilative capacity of the atmosphere. Environ Monit Assess 166:11–27. https://doi.org/10.1007/s10661-009-0981-y

Gocheva-Ilieva SG, Ivanov AV, Voynikova DS, Boyadzhiev DT (2014) Time series analysis and forecasting for air pollution in small urban area: an SARIMA and factor analysis approach. Stoch Environ Res Risk Assess 28:1045–1060

Guerreiro CBB, Foltescu V, de Leeuw F (2014) Air quality status and trends in Europe. Atmos Environ 98:280–291

Han SQ, Bian HX, Yi Y (2007) Research on characteristics of air Pollution in Tianjin. Meteorol Sci and Tech 35:787–791

Han S, Bian H, Tie X, Xie Y, Sun M, Liu A (2009) Impact of nocturnal planetary boundary layer on urban air pollutants: measurements from a 250-m tower over Tianjin, China. J Hazard Mater 162:264–269. https://doi.org/10.1016/j.jhazmat.2008.05.056

Honoré C, Rouil L, Vautard R (2008) Predictability of European air quality: assessment of 3 years of operational forecasts and analyses by the PREV'AIR system. J Geophys Res 113:4302–4310

Hu Q (1997) Notes and correspondence on the uniqueness of the singular value decomposition in meteorological applications. J Clim 10:1762–1766

Kang N, Gao QX, Wand YS, Xin JY, Lin YY, Su FQ (2009) Analysis of regional pollution process and application of system cluster method. Res Environ Sci 22:1120–1127

Kassomenos P, Papaloukas C, Petrakis M, Karakitsios S (2008) Assessment and prediction of short term hospital admissions: the case of Athens, Greece. Atmos Environ 42:7078–7086

Kim JH, Na S, Martin RV, Seo KH, Newchurch MJ (2008) Singular value decomposition analyses of tropical tropospheric ozone determined from TOMS. Geophys Res Lett. https://doi.org/10.1029/2008GL033690

Kuo YM, Chiu CH, Yu HL (2015) Influences of ambient air pollutants and meteorological conditions on ozone variations in Kaohsiung, Taiwan. Stoch Environ Res Risk Assess 29:1037–1050

Li Y (2009) The space-time variations of PM_{10} concentration in major cities of China during 2000–2007. J Arid Land Resour Environ 23:51–54

Li J, Heap AD (2008) A review of spatial interpolation methods for environmental scientists geoscience Australia record 2008/23, p 154. http://corpdata.s3.amazonaws.com/68229/Rec2008_023.pdf

Li JB, Wang JL (2013) An analysis of air quality characteristics of Chongqing (2001–2011). J Southwest Univ (Natural Science Edition) 35:145–153

Li XF, Zhang MJ, Wang SJ, Zhao AF, Ma Q (2012) Variation characteristics and influencing factors of air pollution index in China. Environ Sci 33:1937–1943

Li MS, Zhang JH, Zhang YJ, Zhou L, Li Q, Chen YH (2013) Spatio-temporal pattern changes of ambient air PM_{10} pollution in China from 2002 to 2012. Acta Geogr Sin 68:1504–1512

Li L, Liu M, Fang SD, Xiao Y, Xiang H, Gao ZX, Ye LM, Guo GF (2014) Analysis of meteorological factors of heavy haze in Hubei province during January, 2013. Environ Sci Tech 37:16–20

Liu YQ (2003a) Spatial patterns of soil moisture connected to monthly-seasonal precipitation variability in a monsoon region. J Geophys Res 108(D22):8856. https://doi.org/10.1029/2002JD003124

Liu YQ (2003b) Prediction of monthly-seasonal precipitation using coupled SVD patterns between soil moisture and subsequent precipitation. Geophys Res Lett 30(15):1827. https://doi.org/10.1029/2003GL017709

Liu YQ (2005) Atmospheric response and feedback to radiative forcing from biomass burning in tropical South America. Agric For Meteorol 133:40–57

Liu XH, Zhu B, Wang HL, Zhang EH (2011) Haze variations over 1980–2009 and connecting factors over the Yangtze River Delta Region. China Environ Sci 33:1929–1936

Liu YQ, Goodrick SA, Heilman WE (2013) Wildland fire emissions, carbon, and climate: wildfire-climate interactions. For Ecol Manag 317:80–96. https://doi.org/10.1016/j.foreco.2013.02.020

Ma J, Xu XH, Lin PF (2015) Meridional position biases of East Asian subtropical jet stream in CMIP5 models and their relationship with ocean model resolutions. Int J Climatol. https://doi.org/10.1002/joc.4256

Marlier ME, DeFries RS, Voulgarakis A, Kinney PL, Randerson JT, Shindell DT, Chen Y, Faluvegi G (2013) El Niño and health risks from landscape fire emissions in southeast Asia nature climate change 3(2):131–136

Murray CJL, Majid E, Abraham DF, Stephen L, Rafael L, Catherine M, Mohsen N, Joshua AS, Kenji S, Theo V, Daniel W, Alan DL (2012) GBD 2010: design, definitions, and metrics. Lancet 380:2063–2066. https://doi.org/10.1016/S0140-6736(12)61899-6

Nalder IA, Wein RW (1998) Spatial interpolation of climate normals : test of a new method in the Canadian boreal forest. Agric For Meteorol 92:211–225

Peterson TC, Karl TR, Kossin JP, Kunkel KE, Lawrimore JH, McMahon JR, Vose RS, Yin XG (2014) Changes in weather and climate extremes: state of knowledge relevant to air and water quality in the United States. J Air Waste Manag Assoc 64:184–197. https://doi.org/10.1080/10962247.2013.851044

Ren ZH, Su FQ, Gao QX, Lu SQ, Hong ZX, Hu F, Zhang MG, Lei T (2005) Analysis of the serious atmospheric pollution event caused by emissions in boundary layer. Chin J Atmos Sci 29:57–63

Ren WX, Xue B, Zhang L, Ma ZX, Geng Y (2013) Spatiotemporal variations of air pollution index in China's megacities. Chin J Ecol 32:2788–2796

Rohdel RA, Muller RA (2015) Air pollution in China: mapping of concentrations and sources. PLOS ONE. https://doi.org/10.1371/journal.pone.0135749

Seo J, Youn D, Kim JY, Lee H (2014) Extensive spatiotemporal analyses of surface ozone and related meteorological variables in South Korea for the period 1999–2010. Atmos Chem Phys 14:6395–6415. https://doi.org/10.5194/acp-14-6395-2014

Shahraiyni HT, Sodoudi S (2016) Statistical modeling approaches for PM_{10} Prediction in urban areas; a review of 21st-century studies. Atmosphere 7:15. https://doi.org/10.3390/atmos7020015

Shi TT, Liu YQ, Zhang LB, Hao L, Gao ZQ (2014) Burning in agricultural landscapes: an emerging natural and human issue in China. Landscape Ecol 29:1785–1798

Sofiev M, Siljamo P, Valkama I, Ilvonen M, Kukkonen J (2006) A dispersion modelling system SILAM and its evaluation against ETEX data. Atmos Environ 40:674–685. https://doi.org/10.1016/j.atmosenv.2005.09.069

Stadlober E, Hörmann S, Pfeiler B (2008) Quality and performance of a PM_{10} daily forecasting model. Atmos Environ 42:1098–1109. https://doi.org/10.1016/j.atmosenv.2007.10.073

Susan LR, Christopher JM (2014) Forecasts of seasonal stream flow in West-Central Florida using multiple climate predictors. J Hydrol 519:1130–1140

Tai APK, Mickley LJ, Jacob DJ (2010) Correlations between fine particulate matter ($PM_{2.5}$) and meteorological variables in the United States: implications for the sensitivity of $PM_{2.5}$ to climate change. Atmos Environ 44:3976–3984

Tan J, Zhang Y, Ma WC, Yu Q, Wang Q, Fu QY, Zhou B, Chen JM, Chen LM (2016) Evaluation and potential improvements of WRF/CMAQ in simulating multi-levels air pollution in megacity Shanghai, China. Stoch Environ Res Risk Assess. https://doi.org/10.1007/s00477-016-1342-3

Tao H, Fraedrich K, Menz C, Zhai J (2014) Trends in extreme temperature indices in the Poyang Lake Basin, China. Stoch Env Res Risk Assess 28:1543–1553. https://doi.org/10.1007/s00477-014-0863-x

Tao L, Zhou YT, Li RF (2016) Characteristics of haze days and air pollution index (API) and their relationship with weather conditions at four large cities/districts of China. Trans Atmos Sci 39:110–125

Tian L, Lu RY, Xing WT, Wang L, Wang X, Wang W, Wang JF (2005) Studies on city ambient air quality in China during 2001–2004. J Arid Land Resour Environ 19:101–105

UN (United Nations Economic and Social Commission for Asia and the Pacific) (2001) Air quality in Asia and the Pacific: an analysis in relation to national and international standards, United Nations Publications, 2001 - Air - 113 pages. Book News Inc., Portland

Wallace JM, Smith C, Bretherton CS (1992) Singular value decomposition of wintertime sea surface temperature and 500-mp height anomalies. J Clim 5:561–576

Wang C, Li D (2012) Analysis of the interannual variation of the summer precipitation over the Yellow River basin and the effect factors based on MTM-SVD method. Chin J Atmos Sci 36:823–834

Wang TJ, Hu ZY, Xie M, Zhang Y, Xu CK, Chao ZH (2004) Atmospheric sulfur deposition onto different ecosystems over China. Environ Geochem Health 26:169–177

Wang F, Chen DS, Cheng SY, Li JB, Li MJ, Ren ZH (2010) Identification of regional atmospheric PM_{10} transport pathways using HYSPLIT, MM5-CMAQ and synoptic pressure pattern analysis. Environ Model Softw 25:927–934. https://doi.org/10.1016/j.envsoft.2010.02.004

Wang R, Wu L, Wang C (2011) Typhoon track changes associated with global warming. J Clim 24:3748–3752

Wang J, Qiu C, Liu HB, Cao J, Wang DC, Dong XG (2013) Characteristics of air quality and the correlation between API and meteorological elements in major cities of Shan Dong province. Ecol Environ Sci 22:644–649

Wang H, An J, Shen L, Zhu B, Pan C, Liu Z, Liu X, Duan Q, Liu X, Wang Y (2014a) Mechanism for the formation and microphysical characteristics of submicron aerosol during heavy haze pollution episode in the Yangtze River Delta, China. Sci Total Environ 490:501–508. https://doi.org/10.1016/j.scitotenv.2014.05.009

Wang W, Maenhaut W, Yang W, Liu X, Bai Z, Zhang T, Claeys M, Cachier H, Dong S, Wang Y (2014b) One-year aerosol characterization study for $PM_{2.5}$ and PM_{10} in Beijing. Atmos Pollut Res 5:554–562

Wei YX, Tong YQ, Yin Y, Chen K (2009) The variety of main air pollutants concentration and its relationship with meteorological condition in Nanjing city. Trans Atmos Sci 32:451–457

WHO (2014) Air quality deteriorating in many of the world's cities http://www.who.int/mediacentre/news/releases/2014/air-quality/en/

Wu HB, Wu L (2010) Methods for diagnosing and forecasting climate variability. China Meteorological Press, Beijing, 371 pp

Yang YQ, Wang JX, Gong SL, Zhang XY, Wang H, Wang WQ (2016) PLAM-a meteorological pollution index for air quality and its applications in fog-haze forecasts in North China. Atmos Chem Phys 16:1353–1364. https://doi.org/10.5194/acp-16-1353-2016

Yao HR, Li DL (2013) The relationship between Asian jets and the winter monsoon and their impact on climate in China. Acta Meteorol Sin 71:429–439

Yao SX, Huang Q, Zhao C (2016) Variation characteristics of rainfall in the pre-flood season of South China and its correlation with sea surface temperature of Pacific. Atmosphere 7:5. https://doi.org/10.3390/atmos7010005

Yu B, Huang C, Liu Z, Wang H, Wang L (2011) A chaotic analysis on air pollution index change over past 10 years in Lanzhou, northwest China. Stoch Environ Res Risk Assess 25:643–653. https://doi.org/10.1007/s00477-011-0471-y

Zekri H, Mokhtari AR, Cohen DR (2016) Application of singular value decomposition (SVD) and semi-discrete decomposition (SDD) techniques in clustering of geochemical data: an environmental study in central Iran. Stoch Env Res Risk Assess 30:1947–1960

Zhan W, Zhang Y, Ma W, Yu Q, Chen L (2013) Estimating influences of urbanizations on meteorology and air quality of a Central Business District in Shanghai, China. Stoch Environ Res Risk Assess 27:353–365. https://doi.org/10.1007/s00477-012-0603-z

Zhang PB, Guan ZY, Cai JX (2010) Impacts of inter annual variations of Australian high on the summer temperature in China by SVD analysis. Trans Atmos Sci 33:58–66

Zhang Y, Bocquet M, Mallet V, Seigneur C, Baklanov A (2012) Real-time air quality forecasting, part I: history, techniques, and current status. Atmos Environ 60:632–655

Zhang XL, Tang YX, Xiong YJ, Zhang RJ, Meng W, Cao XY (2014) Analysis and numerical forecast of a regional for-haze in North China plain. J Univ Chin Acad Sci 31:337–344

Zhang LB, Liu YQ, Hao L (2016) Contributions of open crop straw burning emissions to $PM_{2.5}$ concentrations in China. Environ Res Lett 11:014014

Zhu B, Wang HL, Shen LJ, Kang HQ, Yu XN (2013) Aerosol spectra and new particle formation observed in various seasons in Nanjing. Adv Atmos Sci 30:1632–1644. https://doi.org/10.1007/s00376-013-2202-4